Solar Physics with Radio Observations, Proceedings of Nobeyama Symposium 1998, NRO Report 479

Radio and X-ray Observations of the Flares Caused by Interacting Loops

Yoichiro Hanaoka
Nobeyama Radio Observatory, NAOJ,
Nobeyama, Minamimaki, Minamisaku, Nagano 384-1305, Japan
E-mail: hanaoka@nro.nao.ac.jp

Abstract

Interaction between two loops, one of which is a small, newly emerging loop, and another one of which is a large overlying loop, is a typical cause of solar flares and related active phenomena. We revealed the configuration of an emerging loop and an overlying loop using microwave and soft X-ray observations of the flares, along with their magnetograms. Two of the footpoints of the loops, one from the emerging loop and the other from the overlying loop, are included in a single magnetic polarity patch. The two loops form a 'three-legged' structure, and the magnetic field has a 'bipolar + remote unipolar' structure. Relative timing analysis of the brightness of the microwave and hard X-ray sources based on the high-temporal resolution data shows that the brightness fluctuation of the remote source is delayed by 400–600 ms to that of the main source, which is located at the interacting region of the two loops. This is the evidence that the electron acceleration site is located at the interaction region of the two loops.

Key words: Sun: flares — Sun: emerging flux — Sun: high-energy electrons

1. Introduction

Flux emergence eventually causes a collision between the emerging loop and an overlying loop, and interaction between these two loops is one of the well-known typical conditions to cause various active phenomena such as flares, microflares, jets, and surges. We call the loop topology consisting of an emerging loop and an overlying loop, a 'double-loop configuration'. The results of the observational study of the flares and various active phenomena occurring in the double-loop configuration with the Nobeyama Radioheliograph, *Yohkoh*, and ground-based instruments are published by Hanaoka (1996 and 1997; hereafter Papers I and II). In this paper, we review the results in the above papers and also describe new results obtained from the analysis of the high temporal-resolution data.

We survey flares which are considered to occur under the double-loop configuration, and analyzed more than 10 flares. Figure 1 shows a schematic view of the interacting loops under the double-loop configuration. In section 2, the magnetic configuration of the two loops inferred from the observations of the flares are described. The relation between the magnetic configuration and various active phenomena are also briefly mentioned. In section 3, the electron acceleration site of the flares inferred from the analysis of the high-temporal resolution data is discussed.

2. Configuration of Flare Loops

Images of a typical example of the flares occurring under the double-loop configuration, the 1993 June 7 flare, are shown in figure 2. This flare shows common characteristics of the analyzed flares. There are two bright points in microwaves (figure 2a), which are connected by a large soft X-ray loop (figure 2c). The western footpoint of the large loop show an intense brightening in soft X-rays (saturated in figure 2c), and a compact hard X-ray source is also located there. We call it the 'main source', and probably there is a flaring small loop at the main source. On the other hand, the eastern footpoint of the large loop is remarkable only in radio. We call it the 'remote source'. The Hα image (figure 2e) shows a strong brightening at the main source and a compact brightening at the remote source. The large loop becomes bright later in soft X-rays. The time variations of the two radio sources coincide very well, and they show good agreement with the hard X-ray counts of the HXT. Since the distance between the two microwave sources is about 10^5 km, the energy must be transferred by high-energy electrons. Therefore both the main and the remote sources emit microwaves produced by high-energy electrons.

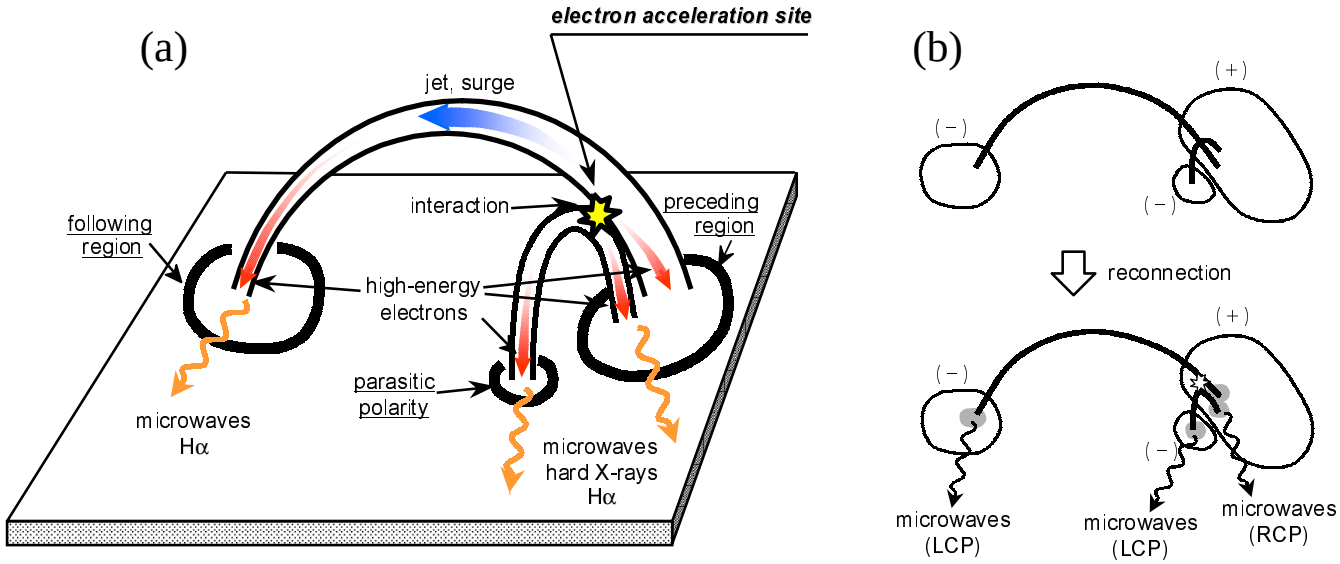

Fig. 1.. (a) Schematic drawing of the double-loop configuration. The two loops show a 'three-legged' structure. The interaction region of the two loops is the origin of high-energy electrons and thermal plasma flows, such as jets and surges. (b) Possible reconnection of the two loops.

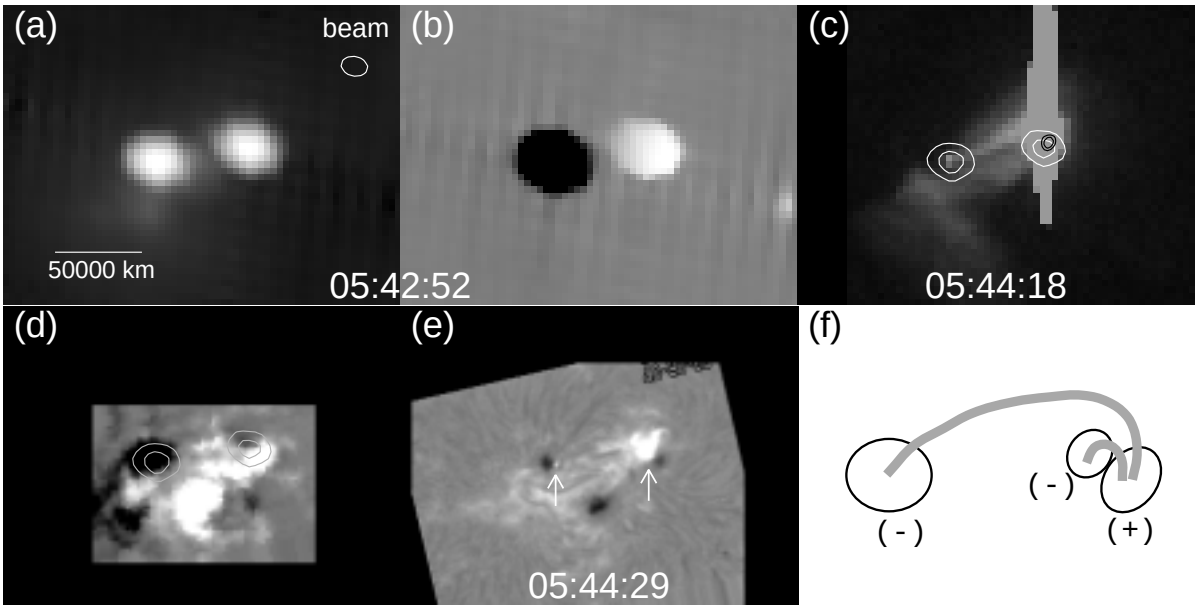

Fig. 2.. Images of the C4.1 flare of 1993 June 7 in NOAA 7518. Each image has a field of view of $5.2' \times 3.9'$, and solar north is to the top. (a)(b) Images of the intensity and the degree of polarization at 17 GHz taken with the Nobeyama Radioheliograph. In the map of the degree of polarization, the right- and left-handed polarizations are displayed in white and black, respectively. (c) Soft X-ray images taken with the SXT on board *Yohkoh* around the peak of the flare, overlaid by white contours showing the microwave image and black contours showing the hard X-ray image of the M1-band (23–33 keV) at 05:43:06 taken with the HXT on board *Yohkoh*. (d) Magnetogram taken with the Stokes Polarimeter of Mees Observatory at 0h UT on June 7. Positive and negative polarities are displayed in white and black, respectively. The contours of the microwave image are overlaid. (e) Hα picture of the flare taken with the Domeless Solar Telescope of Hida Observatory. Hα bright points at the footpoints of the loops are denoted by arrows. (f) Schematic drawing of the relation between the footpoints of the loops and the magnetic polarities.

The main source is observed as a single microwave source, but we presume that the main source actually includes two opposite-polarity microwave sources based on the microwave images and the magnetogram. The degree of polarization in microwaves of the main source has a slope (figure 2b). Such a slope cannot be produced by a single source. Two unresolved microwave sources, which have opposite polarities, can produce a slope in the degree of polarization, even if they merge into a single source in the intensity map. The opposite polarizations correspond to the opposite magnetic polarities. Therefore the slope of the degree of polarization indicates microwave brightening from the two footpoints of a small loop. The magnetogram in figure 2d shows that a parasitic region with negative polarity touches a positive polarity region at the main source. The direction of the positive-negative polarity complex is consistent with the gradient of the degree of polarization. Therefore the microwave observations are consistent with the magnetographic information. The remote source is close to a sunspot (figure 2e) and located in the unipolar region. Therefore, the magnetic field of the flare has a 'bipolar + remote unipolar' structure. Although there are four footpoints associated with the two loops, the magnetic field is not a quadrapole structure. The footpoints are distributed in three magnetic patches, as shown in figure 2f. The small loop and the large one form a 'three-legged' structure. As a result of analyses of many flares, we concluded that the 'bipolar + remote unipolar' magnetic field is a typical structure of interacting loops produced by emerging loops.

In the 'three-legged' structure, the directions of the magnetic fields of two loops are not anti-parallel. Various two-dimensional reconnection models since Heyvaerts, Priest, and Rust (1977) assumed the reconnection between anti-parallel magnetic fields. On the other hand, in three-dimension, quasi-separatrix layers are recently discussed by Démoulin et al. (1996; see also Sakurai 1999), which can be applied to the reconnection between non-anti-parallel loops. Based on their method, Mandrini et al. (1996) proposed a magnetic configuration for an X-ray bright point flare, which was described by van Driel-Gesztelyi et al. (1996). The change of magnetic configuration described by Mandrini et al. (1996) is applicable to our cases, and figure 1b show a possible configuration of the loops in the pre- and the post-flare phases. Aschwanden (1999) reviews recent development of the three-dimensional evolution of the magnetic configuration during flares.

The double-loop configuration is a common source of not only flares, but also microflares, jets, and surges. The double-loop configuration is created by a parasitic polarity region, and the occurrences of the active phenomena and the evolution of the parasitic polarity region are closely related. The parasitic region seen in figure 2d has a lifetime of only one day, and three (micro)flares occur during its evolution. A parasitic region observed in NOAA 7360, of which lifetime is three days, causes many flares and microflares, and half of them are accompanied by jets. There is no activity at the same place before and after the evolution of the parasitic polarity. For the detailed description of the relation between active phenomena and parasitic polarities, see Hanaoka (1998).

3. Electron Acceleration Site

3.1. Timing Difference between the Main and the Remote Sources

Jets and surges, namely thermal plasma flows, are common active phenomena in the double-loop configuration. The high-cadence soft X-ray observations and Hα observations show that jets and surges flow into the large loop from the interaction region of the two loops. This fact means that the thermal plasma originates in the interaction region. If the schematic view in figure 1 is correct, high-energy electrons of the flares are also presumed to originate in the interaction region. Defining the acceleration site of the electrons is very important to study the energy release.

As shown in figure 2, most of the analyzed flares show two sources in microwaves and one hard X-ray source at the main source. These sources are brightened by high-energy electrons. Therefore, the relative timing differences of the brightness variations of these sources give the timing differences of the electron precipitation into these sources. Precise estimation of the timing difference needs high-temporal resolutions because of the much higher speed of the electrons than that of the thermal plasma. The standard data of the Nobeyama Radioheliograph has the time resolution of 1 sec, but the raw data of 50 ms resolution during the flares are cut out from the temporarily storage and kept. Therefore, snapshot images of the flares at 17 GHz can be made in every 50 ms. The HXT has the time resolution of 0.5 s in the flare mode. In most of the analyzed flares, the hard X-ray images show the main source only. Therefore, the hard X-ray total counts can be considered as the brightness of the main source. It is difficult to make hard X-ray images with the 0.5 s resolution because of the insufficient count rate, but this is not a problem in our analysis. The different types of the relative timing studies have been already done by Aschwanden et al. (1995) for the time variations of various energy electrons and Sakao (1994) for the double-footpoint flares.

For the preliminary study, we selected the following three flares,

- 1993 February 6 C5.6 flare

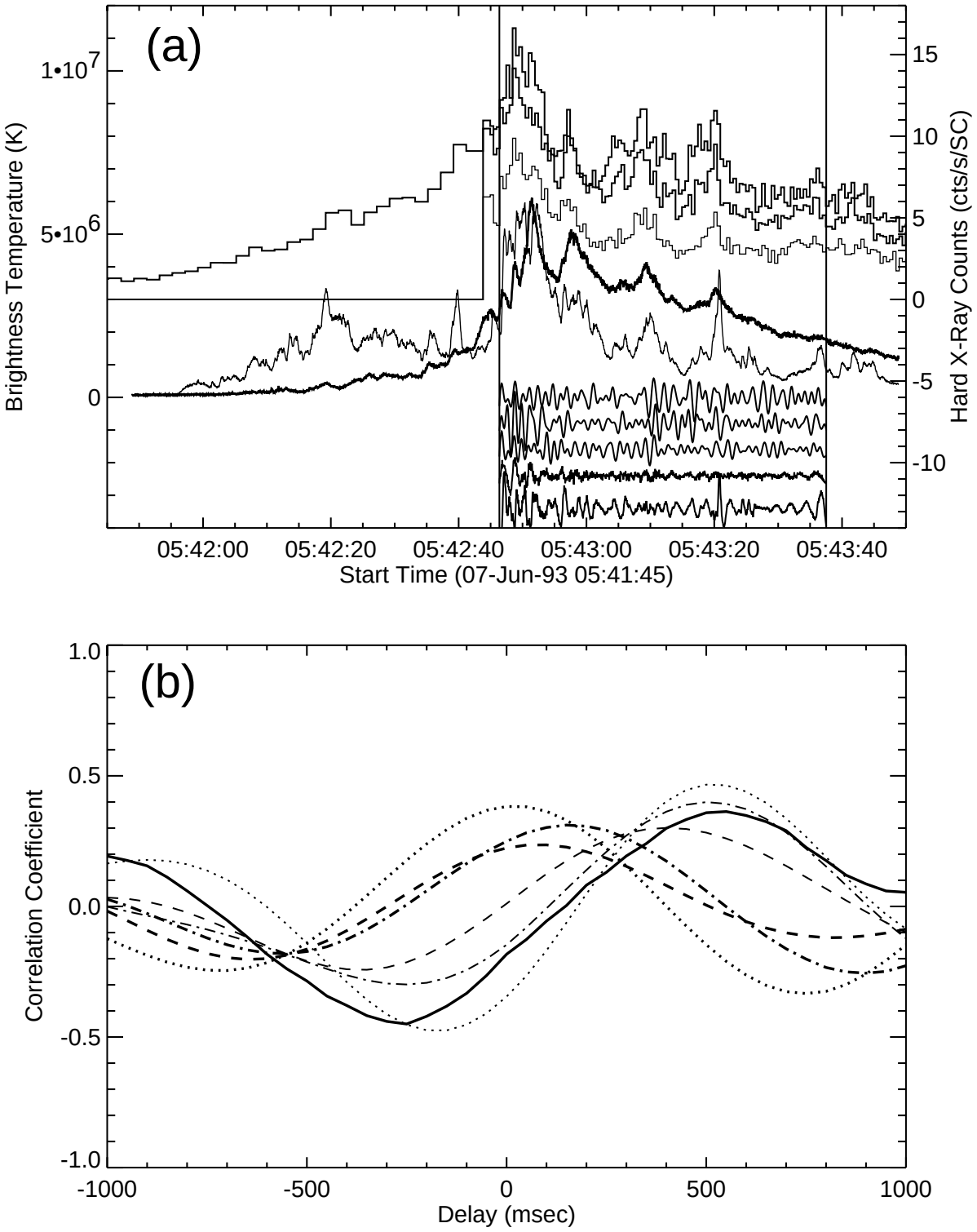

Fig. 3.. High-resolution timing analysis of the radio and hard X-ray brightness changes of the 1993 June 7 flare. (a) The upper part shows the counts of the L/M1/M2 bands of the HXT and the 17 GHz brightness of the main and remote sources, from top to bottom. The lower part shows the fast varying component of these five time-profiles for the 51.2 s (50 ms × 1024) period marked by two vertical lines in the figure. (b) Relation between the assumed delay and the correlation coefficient between two of the fast varying components of the five time-profiles. Thick dotted/dashed/dash-dotted lines show the correlation coefficients between the L/M1/M2 bands of the HXT and the 17 GHz main source, thick solid line shows that between the main and the remote sources at 17 GHz, and thin dotted/dashed/dash-dotted lines show that between the L/M1/M2 bands of the HXT and the 17 GHz remote source.

- 1993 April 10 C9.1 flare
- 1993 June 7 C4.1 flare,

in which the rapid fluctuation of the brightness is remarkable. We show the result of the analysis for the 1993 June 7 flare in figure 3 as an example. The upper part of figure 3a shows the total counts of hard X-rays in the L/M1/M2-bands of the HXT and the radio brightness of the main and the remote sources. We cut out a period of 50 ms × 1024 as shown in figure 3a, when the HXT is in the flare mode and the count rates are high, for our analysis. Rapid fluctuation is clearly seen, and the 0.5 s resolution of the HXT barely resolves the minor peaks. Such a fast and ragged brightness variation suggests that the electrons are accelerated in a short time. The major peaks in radio and hard X-ray time profiles roughly correspond to each other, but one-to-one correspondence of the minor peaks is not clear. Though the time profiles of two sources are expected to shift due to the difference of the distances between the acceleration site and the sources, the time profiles cannot be interpreted so straightforward. The trap of the electrons in the loops and the slight change of the electron precipitation site during the flare probably makes slowly varying component. Then, firstly we remove the slowly varying component, of which frequency is lower than a cutoff frequency, by Fourier filtering from the time profiles. The lower part of figure 3a shows the fast varying component of the radio and hard X-ray time profiles of which frequency is higher than the cutoff frequency of 20. The frequency 20 means that the wave number included in the 50 ms × 1024 period is 20. We calculated the cross-correlation coefficients between two of these fast varying components for various delay values. If two of the fast varying component show the same fluctuation except a certain delay, the cross correlation coefficient becomes the maximum when the correct delay is assumed. The result is shown in figure 3b.

The three curves of which peaks are around zero delay show the correlation coefficients between the L/M1/M2 bands of hard X-rays and the radio main source. Therefore, the hard X-ray and the radio emission from the main source synchronize well, and there is no delay between them. This fact means the fast fluctuation in hard X-rays and that in microwaves of the main source are produced by the same electrons. On the other hand, the correlation coefficient between the main source and the remote source show much different behavior. All the correlation coefficient between the main source (the L/M1/M2 bands of hard X-rays and 17 GHz) and the remote source (17 GHz) become peak around 500–600 ms delay. This fact means that the fast brightness variation of the remote source is similar to that of the main source, but it is delayed by about 500–600 ms. The same results are obtained for the various cutoff frequencies, except too low and too high cutoff frequencies. Furthermore, all the three flares analyzed gives the same results; the variations of hard x-ray and radio brightness of the main source synchronize well, and the remote source is delayed by 400–600 ms to the main source. This result means that the electron acceleration site is far from the remote source, and close to the main source. Therefore, it is most presumable that the interaction region of the two loops is the acceleration site.

Aschwanden et al. (1996) estimate the distance between the electron acceleration site and the hard X-ray source for many flares, including the 1993 June 7 flare shown in figures 2 and 3 on the basis of the electron time-of-flight measurements of hard X-ray data taken with the Burst and Transient Source Experiment (BATSE) on board the Compton Gamma Ray Observatory (CGRO). Their result of the distance between the acceleration site and the hard X-ray source is only about $7.2 \pm 3.4 \times 10^3$ km, and therefore, the acceleration site is very close to the main source. This is consistent with our result, and also suggests that the acceleration site is the interaction region.

3.2. Energy of Electrons

The average length of the large loop connecting the main and remote sources for the three flares is estimated to be about 100000 km (a semi-circular loop is assumed). The average delay of the remote source is about 500 ms. These values gives the typical velocity of electrons to be 2×10^5 km s^{-1}. This velocity corresponds to the energy of electrons of 170 keV. Such energy estimation gives the lower limit, because the actual flight length of the electrons is longer due to the gyration of the electrons around the magnetic field line. If we assume uniform distribution of the pitch angle at the interaction region, where the magnetic field is much stronger than the top of the large loop, the electron flight length is about 30 % longer than the loop length (The detailed description will be given in the forthcoming paper). Considering this factor, we get the velocity and the energy of electrons to be 2.6×10^5 km s^{-1} and 510 keV, respectively.

Some radio observations have shown the delayed brightenings at the remote site with the energy transfer velocity of about 10^5 km s^{-1} before the pitch angle correction (Nakajima et al. 1985, Lang and Willson 1989, Willson et al. 1993). These observations including ours are the direct measurement of the velocities of electrons which precipitate into the remote radio sources.

4. Conclusions

We obtained the following conclusions from the study of the radio, X-ray, and optical observational data of the flares and various active phenomena occurring in the double-loop configuration.

(1) The magnetic configuration of the two loops, one of which is an emerging loop, and another one of which is an overlying, pre-existing loop, is revealed to be a 'bipolar + remote unipolar' structure. Therefore, the two magnetic loops forms a three-legged structure. In this configuration, the magnetic field of the two-loops is not anti-parallel. This is one of the typical configurations which causes active phenomena, such as flares, microflares, jets, and surges.

(2) The high-energy electrons in the flares in the double-loop configuration are accelerated in the interaction region of the two loops. Thermal plasma flows (jets and surges) are known to originate in the interaction region. Therefore, the interaction region is the source of both the thermal plasma flows and the non-thermal high-energy electrons. The interacting loop model is appropriate to both the non-thermal and the thermal phenomena.

The author expresses his hearty thanks to Mees Solar Observatory of the University of Hawaii, for providing the magnetograph data. The magnetograms of Mees Solar Observatory were produced with the support of NASA grant NAGW-1542 and NASA contract NAS8-37334. Hida Observatory of Kyoto University provided the Hα pictures.

References

Aschwanden, M. J., Schwartz, R. A., and Alt, D. M.: 1995, ApJ 447, 923
Aschwanden, M. J., Kosugi, T., Hudson, H. S., Wills, M. J., and Schwartz, R. A.: 1996, ApJ 470, 1198
Aschwanden, M. J.: 1999, in these proceedings
Démoulin, P., Hénoux, J. C., Priest, E. R., and Mandrini, C. H.: 1996, A&A 308, 643
Hanaoka, Y.: 1996, Sol. Phys. 165, 275 (Paper I)
Hanaoka, Y.: 1997, Sol. Phys. 173, 319 (Paper II)
Hanaoka, Y.:1998, in Coronal Jets and Plumes, ESA SP-421, ed. T.-D. Guyenne (ESA/ESTEC, Noordwijk) p171
Heyvaerts, J., Priest, E. R., and Rust, D. M.: 1977, ApJ 216, 123
Lang, K. R. and Willson, R. F.: 1989, ApJL 344, L77
Mandrini, C. H., Démoulin, P., van Driel-Gesztelyi, L., Schmieder, B., Cauzzi, G., and Hoffman, A.: 1996, Sol. Phys. 168, 115
Nakajima, H., Dennis, B. R., Hoyng, P., Nelson, G., Kosugi, T., and Kai, K.:1985, ApJ 288, 806
Sakao, T.:1994, PhD Thesis, The University of Tokyo
Sakurai, T.:1999, in these proceedings
van Driel-Gesztelyi, L., Schmieder, B., Cauzzi, G., Mein, N., Hofmann, A., Nitta, N., Kurokawa, H., Mein, P., and Staiger, J.: 1996, Sol. Phys. 163, 145
Willson, R. F., Lang, K. R., and Gary, D. E.: 1993, ApJ 418, 490